bioresources.com

The Establishment and Numerical Calculation of a Heat Transfer Model of a Graphene Heating Energy Storage Floor

Chunmei Yang, Bo Guan, Zihao Zhang, Jiawei Zhang,* Bo Xue, and Xinchi Tian

A new type of graphene electric heating solid wood composite floor and its heat transfer model were designed to enable users to have a higher-quality and safe living experience. A heat transfer mathematical model was developed. The structural entity of the composite graphene heating floor was drawn using Solidworks software. The floor structure was abstracted as a two-dimensional model using MATLAB software to obtain the temperature rise curves and corresponding time of each group. Then, six groups of the best data were selected from the experimental data to simulate the heat storage capacity of graphene floors. The optimal group of the model was verified *via* experiments. According to the simulation, the comprehensive performance was optimal when the overall thickness of the floor was 18 mm, the thickness of the floor surface was 4 mm, and the thickness of the heat-accumulating layer was 2 mm. The experimental results showed a maximum difference between the measured and calculated data of only 3.2%, which shows the scientific validity, accuracy, and advancement of the model. The composite graphene electric heating energy storage floor designed in this study can be regarded as safe, reliable, environmentally friendly, and healthy.

*Contact information: College of Mechanical and Electrical Engineering, Northeast Forestry University, Harbin 150040 China; *Corresponding author: 1006702680@qq.com*

INTRODUCTION

With the progress and development of science and technology, the requirements of people in terms of quality of life are getting higher and higher. Particularly for heating in winter, reaching the temperature standard is only the basic guarantee for people, and the household heating industry needs to meet the requirements of comfort and energy savings at the same time. In recent years, electrically heated floor, which has the characteristics of low energy consumption, rapid temperature increase, and high environmental comfort, has begun to flourish. Graphene floor has the characteristics of good thermal insulation effect, strong energy storage performance, and high environmental comfort of traditional floors. In addition, floor radiant heating enables the users to adjust the temperature themselves and the temperature increases faster compared with traditional heating methods, *e.g.*, air conditioner and water heating.

Under the working mode of strong convection heat exchange by blowing high-temperature air out of the air conditioner, the hot air will blow onto the body directly, resulting in a lack of sufficient comfort of the users, and the air temperature above is higher

than the temperature below due to the thermal expansion of the hot air during the working process, resulting in a hot head and cold feet, which is contrary to the appropriate health preservation law of the human body. However, the far-infrared wavelength produced by a graphene electrically-heated floor is similar to that of the human body. Thus, the human body can receive more far-infrared radiation and produce a certain resonance. This can promote human blood circulation and metabolism and has an obvious physiotherapeutic effect. Furthermore, the heat generated under a stable working state heats the air upward from the floor surface, showing a temperature gradient of "warm feet and cool head", which can create a comfortable feeling.

A new type of composite material, involving graphene, has received extensive attention from many international scholars due to its excellent thermodynamic and electrical properties. Graphene is a two-dimensional structure material of carbon atoms connected by sp2 hybridization. Due to the presence of unbonded orbital electrons in its structure, graphene's electrons can move freely, with a carrier mobility of 20000 $cm^2/(V \cdot s)$. It has the lowest resistivity among the known materials, making it have good conductivity and thermal conductivity (Echeberria *et al.* 2012). Song (2019) constructed a three-dimensional graphene material and applied it to the preparation of electrothermal film. During the experiment, graphene oxide was first prepared by the Hummers method, and then graphene electrothermal film was prepared by self-assembly method. It was found that the film could heat up to 183 ℃ when applied with 15 V direct current. The application of high temperature heating of electric heating film was realized, which opens new ideas for the field of heating materials (Song 2019). A graphitic nano sheet electrothermal film was prepared by Liu (2017), and its electrothermal properties were studied. The test results showed that the temperature of the prepared nano graphite sheet/waterborne polyurethane (GNP/WPU) composite electric heating floor can be stabilized at 78 ℃, and the temperature difference between left and right was within 3 ℃, which has high practical application value.

Professor Mazumder of the University of Michigan in the United States studied the convection model by using the numerical model of multi-channel and multi-layer heat transfer and molten pool convection, which plays an important role in understanding the solidification texture of graphene under different laser scanning modes. The method of computer simulation and experiment was used to simulate and verify the heat transfer and physical changes of molten pool of multilayer materials with different laser scanning modes, which has important scientific value for the preparation of graphene multilayer materials (Wei *et al*. 2015). Vivekchand *et al*. (2008) prepared graphene/epoxy resin composites. The research showed that when the content of graphene was 25%, the thermal conductivity of the composites can reach 6.44 W/m·K, which represents an increase by 3000%. The addition of graphene into the polymer body is not only conducive to the improvement of the electrical properties and thermal conductivity of the polymer matrix, but also of great significance for the enhancement of the glass transition temperature and mechanical properties of the composite (Vivekchand *et al.* 2008). Al-Mashaal *et al.* (2017) prepared a kind of electric actuator based on electrically driven and mechanically vibrated graphene/polymethylmethacrylate (PMMA) bilayer structure by using bilayer materials with different mechanical and thermal properties. These materials can cause mechanical vibration of the film structure under the electric heat conduction mechanism. When AC and DC voltages are applied to the drive metal electrode, Joule heat will cause the local temperature of the material to rise, resulting in physical expansion and current drive.

Chen *et al.* (2016) prepared highly conductive graphene films by means of electrification, heating, and reduction. The conductivity was up to 3112 S/cm, and the square resistance was lower than 0.8 Ω/sq. This is because the Joule heat energy generated by electrification reaches 2750 K, which can remove the remaining oxygen-containing groups and other defects on the RGO surface and improve its regularity. With the increase of applied voltage, the current density increases gradually. When the electric field reaches 6.55 V/mm, the current density changes from 0.0033mA/ μm^2 and suddenly increases to 0.76 mA/ μm^2. During the electrothermal performance test, as the Joule heat increased to 2500 K, the resistance showed a linear downward trend, and then it tended to be stable. After the electrothermal test, the RGO film has a closer contact between graphene sheets due to the removal of oxygen-containing groups, and its surface became smoother, with a thickness of 1.25 μm reduced to 1.03 μm (Chen *et al.* 2016). In addition, the emissivity of the graphene material can reach above 0.92. The cited authors sprayed the graphene dispersion using a spray gun, and then the layer was dried at 80 °C for 1 h to prepare the graphene coating. The effects of coating thickness, jet pump pressure, and nozzle size on the thermal conductivity were evaluated during the test. The results show that the coating was able to enhance the thermal conductivity and heat transfer rate, and it exhibited excellent snow melting and deicing efficiency. Therefore, graphene has excellent thermal radiation performance and electrothermal response speed, and it can operate stably at higher temperatures. However, pure graphene needs to be coated on a hard substrate, and its flexibility needs to be further improved. This is helpful for the preparation of flexible electrothermal materials (Chen *et al.* 2017).

Wang *et al*. (2017) prepared a graphene fiber with high tensile strength and low voltage response. The graphene oxide was reduced with hydrogen iodide, and the picture and infrared thermal image of graphene fiber are shown in Fig. 1. The fracture strain of the graphene fiber was up to 70%, and the conductivity was up to 6 x 10^5 Sm^{-1}, the temperature reached 424 °C within 5 s, and the maximum heating rate reached 571 $°Cs^{-1}$. The electric heating device showed excellent thermal performance and stability. In the research, a braided carbon fiber material was designed, and a small flexible thermal actuator was made, which can stably conduct heat in a large bending state (Wang *et al.* 2017).

Al-Mashaal *et al.* (2017) prepared a kind of electric actuator based on electrically driven and mechanically vibrated graphene/polymethylmethacrylate (PMMA) bilayer structure by using bilayer materials with different mechanical and thermal properties, which can cause mechanical vibration of the film structure under the electric heat conduction mechanism. When AC and DC voltages are applied to the drive metal electrode, Joule heat will cause local temperature of the material to rise, resulting in physical expansion and current drive.
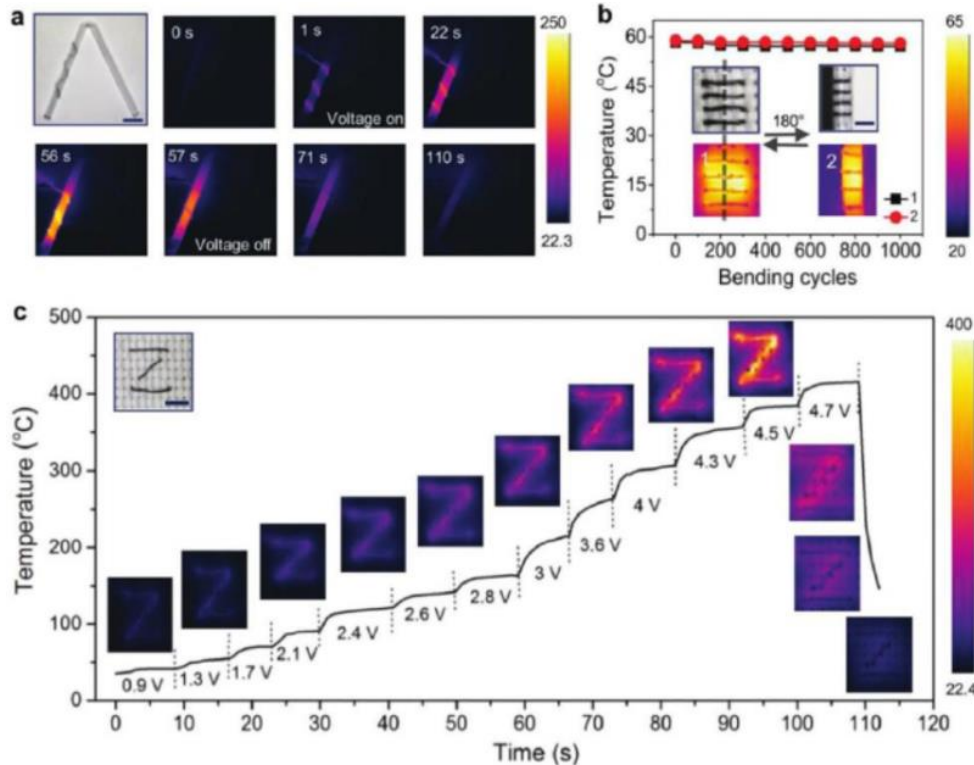
Fig. 1. (a) Photographs and infrared thermograms of graphene fibers; (b) Temperature change of 180° bending recovery of fabric during heating; (c) Infrared thermal image of Z-shaped pattern when the voltage changes from 0.9 to 4.7 V, internal image Z-shaped pattern fabric

The temperature increase rate is one of the more important performance indexes of an electrically heated floor. Most of the existing research results have focused on the establishment of a theoretical model of low-temperature radiant water heating (Hauser *et al.* 2000; Yang *et al.* 2001; Shi 2007; González and Prieto 2021) and the detection of heat storage performance of heating floor (Du *et al.* 2018; Zhou *et al.* 2018; Cao *et al.* 2018; Liu *et al.* 2018) and there is no complete theoretical system for the problem of the temperature increase rate. The thickness of the floor surface, the layout of the heating layer, and the spacing of the heating fiber all affect the electrothermal performance of the floor. As for these problems, in this paper, an electrically heated floor mathematical model was established to describe the floor temperature rise process, a numerical method was used to simulate the temperature distribution inside and on the surface of the floor, and the floor products with good electrothermal performance and heat storage performance were obtained by optimizing the important influence parameters of the floor, which will play a certain guiding role in the electrothermal floor industry.

EXPERIMENTAL

Structural Design of Composite Graphene Heating Floor

A composite graphene heating floor is composed of a floor surface layer, a graphene heating layer, a heat-accumulating layer, a reflective insulation layer, and a floor substrate layer, ordered from top to bottom.

bioresources.*com*

The floor surface layer is in direct contact with the external environment, so wood with excellent thermal conductivity, beautiful texture, and high strength should be selected. However, because the thermal conductivity of wood is small and the difference in thermal conductivity between different woods is not obvious, the density and specific heat capacity will have a greater impact on the overall temperature increase of the floor and show a proportional relationship (Cungen Liu *et al.* 2018). Therefore, in this paper, walnut wood, which has a high density, high specific heat capacity, beautiful texture, and high strength, was considered, along with poplar wood. A moderate comprehensive performance was chosen as the base material, so as to save resources and reduce costs (Luo *et al.* 2012).

The electrically heated medium of a solid wood composite graphene electrically heated floor was comprised of a graphene heating film wrapped with a polymer resin film, which contained graphene fibers, silver plated copper wire, and heat-conducting fibers. Among them, graphene fiber was its primary heating component. After the power turns on, the graphene lattice vibrates and violently collides under the action of an electric field to generate heat energy; the electric heating film transfers the heat to the contacted floor surface *via* means of heat conduction. Then, the temperature of the floor surface increases, transferring the heat to the indoor environment and indoor buildings *via* means of convective heat transfer and radiant heat transfer. The heating core layer of the electric heating film adopts the heating mode of "replacing layer with line", and the graphene is made into strip-shaped heating fibers based on equal spacing. On the premise of ensuring heating uniformity, the fiber spacing was increased as much as possible, so as to save materials and reduce costs.

The heat-accumulating layer is composed of woods with a certain thickness. The woods are natural heat storage materials, which can effectively realize the heat storage function of the floor. The use of solid woods with a certain thickness not only can continuously distribute the stored energy to the environment when the floor is powered off, but it also provides a thermal conductor around the electric heating film during the heating process to increase the transverse heat transfer rate and improve the temperature uniformity within the area of the floor.

Graphene can emit infrared light waves with thermal radiation as the primary heating mode. The coating of aluminum foil film on the lower surface of the heat-accumulating layer can yield a non-electromagnetic radiation surface far-infrared barrier, which can effectively prevent the heat from transferring to the bottom (an approximately 90% reduction). A ceramic aluminum silicate insulation layer was installed under the aluminum foil reflection layer to ensure that the heat was fully preserved in the heat-accumulating layer.

Each floor was connected in parallel through wires. Separately, each floor can be used as an independent heating body, which will eventually gather on the bus. The design is shown in Fig. 2.
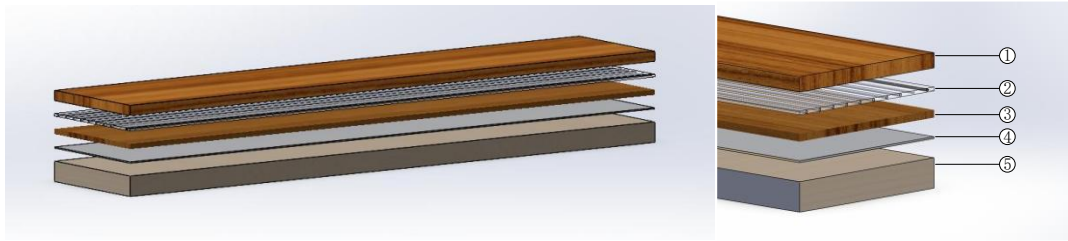
Fig. 2. Layered structure of composite graphene floor (Note: 1: Floor surface layer; 2: Graphene heating layer; 3: Heat-accumulating layer; 4: Aluminum foil reflective layer and ceramic aluminum silicate thermal insulation layer; and 5: Floor substrate layer)

The working conditions occur when the graphene heating layer is powered on to generate heat, and the heat is transmitted upward and downward to the floor surface layer and the heat-accumulating layer. The temperature of the contact part between the floor surface layer and the heating layer increases first, and then the heat is transferred upward to the surface layer. At this time, the floor surface layer carries out convective heat transfer and radiation heat transfer with the outside to transfer the heat to the room. The temperature of the contact part between the heat-accumulating layer and heating layer increases first, and then the energy is transferred downward to the reflective insulation layer. The reflective insulation layer does not absorb the energy and reflects the energy back to the heat-accumulating layer. Then, the heat transferred downward by the heating layer is stored in the heat-accumulating layer. When the energy absorbed by the heat-accumulating layer reaches its limit, it will no longer be absorbed, and all the heat generated by the heating layer will be transmitted to the floor surface layer. According to the thermal engineering principle that hot air is light and cold air is heavy, the heat radiated by the graphene electrically heated floor makes the indoor hot air continuously rise and the cold air continuously decline, replenish, and gradually become heated. By repeating this cycle, the indoor temperature continuously increases, finally achieving the purpose of heating.

Graphene Floor Heat Transfer Model

Physical model and model simplification: Basic assumptions

The heat transfer process of graphene heating floor is a three-dimensional heat conduction process in space, and its heat transfer process is relatively complex. If analyzed in detail, it would deviate from the research topic of this paper. In order to reasonably simplify the calculation, the following assumptions were made for the model:

1) The materials of each floor layer are bonded tightly and correspond to the ideal state, and the contact thermal resistance is ignored.

2) The direction dimension of the graphene heating fiber is much larger than the thickness of the floor surface, which can be assumed to be in a plane strain state. Therefore, a section is taken for overall analysis and research.

3) If any two adjacent graphene heating fibers have the same width, it is assumed that the temperature distribution is consistent and the temperature on both sides of the fiber is symmetrically distributed in the longitudinal direction.

4) The reflective insulation layer has good thermal insulation, and the heat is not transferred downwards. Therefore, it is considered that the reflective insulation layer is an adiabatic surface.

5) The temperature distribution of two adjacent graphene heating fibers is obviously symmetrical relative to the center line of the middle section. Therefore, the middle of any two graphene fibers is a heat balance surface, so it is also an adiabatic surface (Zhang *et al.* 2005).

Schematic diagram of model

The heat transfer problem under the conditions of the floor surface layer and heat-accumulating layer having different thicknesses and graphene heating fibers with different spacing needs to be simulated and calculated in this paper. Therefore, a structure diagram of the graphene heating floor was established (as shown in Fig. 3).

Currently, according to GB/T standard 18103 (2013), the thickness of a multiple solid wood parquet flooring is required to be between 12 and 22 mm, and the common thickness in the market is typically 18 mm. In order to better meet the market requirements and installation habits, the overall thickness of the floor was 18 mm. The floor surface was the surface layer of the floor that directly bears various physical and chemical effects. This work adopted 2 mm as the division unit and used 2, 4, 6, 8, 10 and 12 mm to carry out the calculations. According to the processing technology of the research group, the overall thickness of the heating layer and insulating layer was calculated as 1 mm, and the spacing of the graphene heating fiber was calculated as 5 and 10 mm. The heat-accumulating layer was used to store heat and protect heating equipment, whose thickness is not only related to the heat dissipation of the floor, but also directly affects the continuous heat release. In this paper, 0, 2, 4, 6, 8, 10, 12, 14, and 16 mm were used for calculations. The reflective thermal barrier was provided by the Hebei Obele New Building Materials Co., Ltd, with the overall thickness calculated as 1 mm. The substrate layer primarily ensures the overall mechanical properties and joggle point technology of the floor. Due to the presence of the reflective thermal barrier, the overall thickness shall match the overall upper layer thickness.
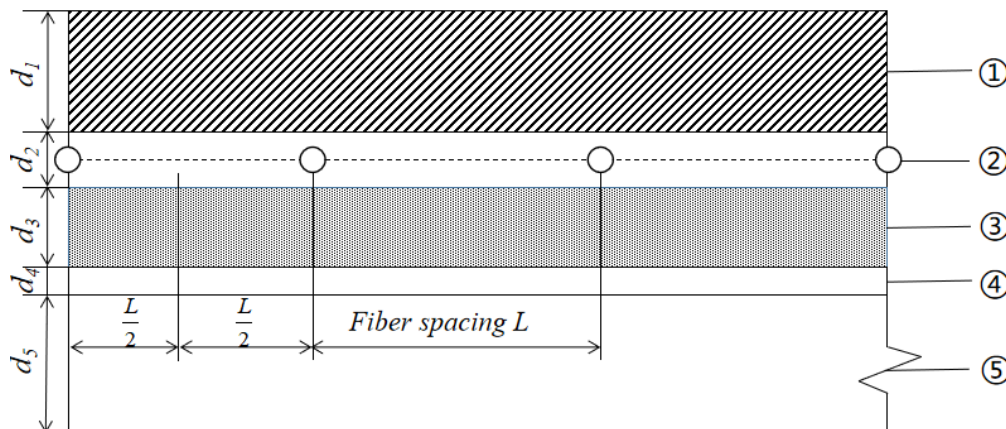

Fig. 3. Structural diagram of graphene heating floor. 1: Floor surface layer; 2: Graphene heating layer and insulating layer; 3: Heat-accumulating layer; 4: Reflective layer and ceramic aluminum silicate thermal insulation layer; 5: Floor substrate layer

Description of the model design parameters

In order to apply the calculated data into the engineering practice, the parameters in Table 1 and the structure of the floor slab covered the actual working conditions as much as possible.

Table 1. Parameter List

Floor Surface	$\lambda_1 = 0.15w/(m \cdot °C)$ $\rho_1 = 496kg/m^3$ $c_1 = 1256J/(kg \cdot °C)$
Thickness of the surface layer (mm)	2, 4, 6, 8, 10, 12, 14, 16, 18
Graphene heating layer (mm)	$P = 2.8w/m^2$ $d^2 = 1$ mm
Graphene fiber spacing (mm)	5, 10
Heat-accumulating layer	$\lambda_1 = 0.15w/(m \cdot °C)$
Heat-accumulating layer (mm)	0, 2, 4, 6, 8, 10, 12, 14, 16

Theoretical Analysis of the Heat Transfer Model

Division of the minimum computing unit

The calculation was for half of the heat transfer units between two heating fibers, as shown in Fig. 4. The finite volume method was used for analysis, and the two-dimensional unsteady heat conduction equation was used to solve the temperature distribution of the calculation element.
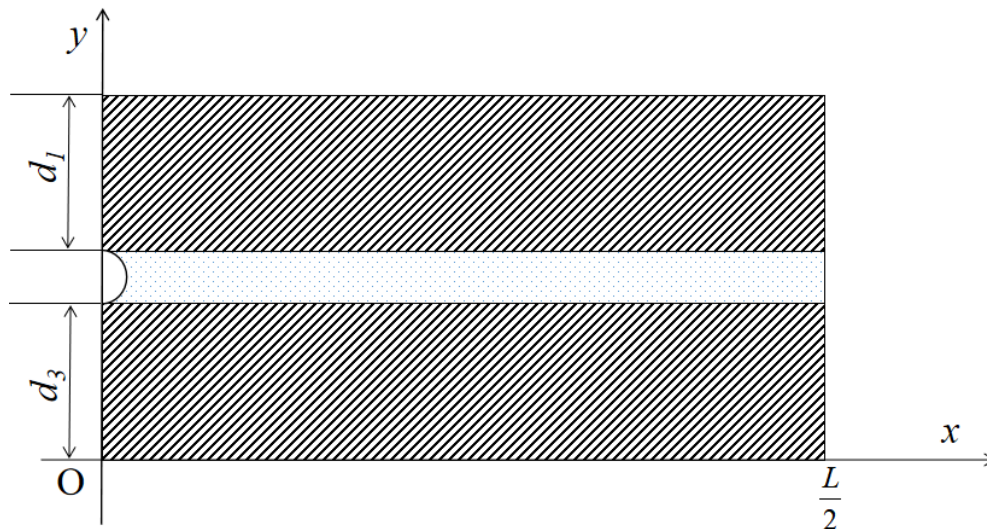

Fig. 4. Minimum calculation unit

The heat transfer equation of the model should be a two-dimensional unsteady heat transfer with one internal heat source (Yang and Tao 2006). The governing equation is shown in Eq. 1,

$$\frac{\partial T}{\partial t} = a\left(\frac{\partial^2 T}{\partial x^2} + \frac{\partial^2 T}{\partial y^2}\right) + \frac{\dot{\varphi}}{\rho c} \tag{1}$$

where the initial condition is $t=0$; $T = T_0$, T is the temperature (°C), t is the time (s), a is the thermal diffusivity (m^2/s), and $\dot{\phi}$ is the generation heat of heat source per unit volume (J).

Boundary condition

During operation, the temperature distribution on both sides of the graphene heating fiber was symmetrical in the graphene fiber. Therefore, the graphene heating fiber could be considered as adiabatic. The temperature distribution of two adjacent graphene heating fibers was obviously symmetrical in the middle section. Therefore, the middle of any two graphene fibers was a thermal equilibrium surface, so it was also an adiabatic surface. Therefore, the boundary conditions were established as shown in Eqs. 2 and 3,

$$x = 0, \frac{dT}{dx} = 0 \tag{2}$$

$$x = \frac{L}{2}, \frac{dT}{dx} = 0 \tag{3}$$

Because the aluminum foil and thermal barrier were attached under the heat-accumulating layer, it was considered that heat was not transferred downward. Therefore, the heat-accumulating layer was an insulating surface when $y = 0$, as shown in Eqs. 4 and 5,

$$y = 0, \frac{dT}{dy} = 0 \tag{4}$$

$$y = d, -\lambda \frac{dT}{dy} = q_r + q_c \tag{5}$$

where q_r is the radiant heat transfer and q_c is the convective heat transfer.

The surface temperature limit of the heat of the graphene floor selected in this article was 40 °C, which was a low-temperature electric heating ground heating method. The heating method of the low-temperature electric heating floor primarily included heat convection and radiant transfer, among which radiant transfer played the leading role.

The radiant transfer of the floor is shown in Eq. 6,

$$q_r = \sigma F_r (T^4 - T_r^4) \tag{6}$$

where σ is the Stefan-Boltzmann Constant (σ), 5.67×10^{-8} W/(m^2·K^4), F_r is the radiation heat transfer constant, T is the heating surface temperature (K), and T_r is the unheated surface temperature (K).

For a box-shaped room with a uniformly heated ceiling, ground, or wall, when other surfaces were another temperature and were ideal scattering surfaces, the famous Van't Hoff Equation could be applied, as shown in Eq. 7,

$$F_r = \frac{1}{\frac{1}{F_{p-r}} + (\frac{1}{\varepsilon_p - 1}) + \frac{A_p}{A_r}(\frac{1}{\varepsilon_r} - 1)} \tag{7}$$

where F_{p-r} is the radiation angle coefficient of the radiant plate to unheated surface, for flat plate $F_{p-r} = 1.0$, A_p is the surface area of heating surface (m^2), A_r is the unheated surface unheated plate area (m^2), ε_p is the radiant plate surface emissivity, and ε_r is the surface emissivity of the unheated plate.

Theoretical analysis of the model

Since only the floor surface generated heat and the surface of the envelop enclosure did not, the emission coefficient of the envelop enclosure was nearly equal. Furthermore,

bioresources.com

the irradiated surface was hardly heated or cooled. At this time, the weighted mean temperature (T_r) was used to represent the temperature of the overall envelope enclosure, as shown in Eqs. 8 and 9,

$$T_r = \frac{\sum_{j \neq p}^{n} A_j \varepsilon_j T_j}{\sum_{j \neq p}^{n} A_j \varepsilon_j} \tag{8}$$

$$T_j = T_n - K \frac{(T_n - T_w)}{9.4} \tag{9}$$

where A_j is the surface area other than the radiant plate (m^2), ε_j is the thermal emissivity except the radiant plate, T_j is the indoor unheated surface temperature (°C), T_n is the indoor temperature (°C), T_w is the outdoor temperature (°C), K is the thermal conductivity of the unheated surface (W/(m^2·°C)), and the surface heat transfer coefficient of the fence structure equaled 9.4 (W/(m^2·°C)).

In fact, the heat reflectivity of the non-reflective surface of the non-metal or paint metal was approximately 0.9 and the radiation coefficient was Fr = 0.87. As such, it was found that $\sigma F_r = 5 \times 10^{-8}$. Thus, the radiation equation for radiant heating and cooling is shown by Eq. 10,

$$q_r = 5 \times [(T + 273)^4 - (T_r + 273)^4] \tag{10}$$

Convection heat transfer on a floor surface during ground heating is shown by Eq. 11,

$$q_c = 2.42 \times \frac{|(T - T_a)|^{0.31}(T - T_a)}{D_e^{0.08}} \tag{11}$$

where D_c is the equivalent diameter of the radiant plate, and $D_c = \frac{4A}{L}$, where A is the plate area (m^2) and L is the plate perimeter (m).

According to the test time made by the research group, the authors found the convective heat transfer is represented by Eq. 12,

$$q_c = 2.75 \times |T - T_a|^{0.31}(T - T_a) \tag{12}$$

Generally, T_a represents the design temperature of the indoor air, which could be approximately considered T_a = AUST when heating on the ground or cooling on a flat roof.

The theoretical overall heat transfer (q_l) could be considered as the sum of the convective heat transfer and radiant heat transfer, as shown in Eq. 13,

$$q_l = q_r + q_c \tag{13}$$

The power of the electric heating film was 280 w/m^2, the thickness was $\delta = 1$ mm, and the heat power was 95%. The heat dissipation efficiency according to the heat production principle of the fin is show in Eq. 14,

$$\eta_f = \frac{\text{Actual heat dissipation}}{\text{Heat dissipation of rib surface at rib base temperature}} \tag{14}$$

where the actual thermal performance of the $D_e = \frac{4A}{L} = \frac{4 \times 0.9 \times 0.114}{2 \times (0.9 + 0.114)} = 0.202367m$ longitudinal fin of the rectangular section is shown in Eqs. 15 through 17,

$$\eta_f = \frac{\frac{hP}{m}\theta_0 th(mH')}{hPH'\theta_0} = \frac{th(mH')}{mH'} \tag{15}$$

bioresources.com

$$m = \sqrt{\frac{2h}{\lambda\delta}} \tag{16}$$

$$H' = H + \frac{\delta}{2} \tag{17}$$

Furthermore, the actual heat release was $q_s = q_l \times q_f$.

Therefore, the heat source item, *i.e.*, the heat energy generated per unit volume per unit time, is shown as Eq. 18,

$$\dot\varphi = \frac{q_s}{\delta} = \frac{280 \times 95\%}{0.001} = 2.66 \times 10^5 w/m^2 \tag{18}$$

where $\dot\varphi$ was a converted heat item, as shown in Eq. 19,

$$\dot\phi = -\frac{\phi_s}{A_c dx} = -\frac{q_s}{\delta} \tag{19}$$

Process and method of model solving

Because the heat transfer model was abstracted from practical problems, it was quite difficult to solve *via* the analytical method. Solving this kind of partial differential equation would also deviate from the primary purpose of this article. This article dealt with the governing equations and boundary conditions *via* discretization, adopted the finite difference method to form a system of linear equations, and solved them by the over-relaxation iterative method (Chengbin Zhang *et al.* 2020). The basic idea of the numerical calculation of the heat-transfer model was to give the calculated object a finite number of nodes in time and space. It adopted the finite differences and finite volume method to set up the algebraic equation of the discrete set of values and obtained the temperature value of the discrete point through solving algebraic equations (Junan Lu 2001).

The governing equation is shown in Eq. 20,

$$T(x_i, y_j, t_n + \Delta t) = T(x_i, y_j, t_n) + \frac{\partial T}{\partial t}(x_i, y_j, t_n) + o(\Delta t^2) \tag{20}$$

Analogical and Euler's methods are shown in Eq. 21.

$$\frac{\partial T}{\partial t}(x_i, y_j, t_n) = a(\frac{\partial^2 T}{\partial x^2} + \frac{\partial^2 T}{\partial y^2}) + \frac{\dot\varphi}{\rho c} \tag{21}$$

Through the discretization of x, the authors were able to obtain Eq. 22,

$$x_i = 0 + (i-1)\Delta_x, among \frac{l}{\Delta_x} = N_x, i = 1,2,\cdots,N_x + 1 \tag{22}$$

and through the discretization of t, the authors were able to obtain Eq. 23,

$$t_n = 0 + (n-1)\Delta_t, among\ t = 1,2,\dots,n+1 \tag{23}$$

From Taylor's expansion, the authors were able to acquire Eqs. 24 and 25,

$$T(x_i + \Delta x, y_j, t_n) = T(x_i, y_j, t_n) + \frac{\partial T}{\partial x}(x_i, y_j, t_n)\Delta x + \frac{1}{2}\frac{\partial^2 T}{\partial x^2}(x_i, y_j, t_n)\Delta x^2 + O(\Delta x^2) \tag{24}$$

$$T(x_i - \Delta x, y_j, t_n) = T(x_i, y_j, t_n) - \frac{\partial T}{\partial x}(x_i, y_j, t_n)\Delta x + \frac{1}{2}\frac{\partial^2 T}{\partial x^2}(x_i, y_j, t_n)\Delta x^2 + O(\Delta x^2) \tag{25}$$

which results in Eq. 26.

$$T_{i,j}^n = T(x_i, y_j, t_n) \tag{26}$$

Combining Eqs. 24 and 25 gives rise to Eq. 27,

$$T_{i+1,j}^n + T_{i-1,j}^n = 2T_{i,j}^n + \frac{\partial^2 T}{\partial x^2}(x_i, y_j, t_n) + O(\Delta x^2) \tag{27}$$

which can be approximated by Eq. 28,

$$\frac{\partial^2 T}{\partial x^2} \approx \frac{T_{i+1,j}^n + T_{i-1,j}^n - 2T_{i,j}^n}{\Delta x^2} \tag{28}$$

Similarly, through the discretization of *y*, the authors were able to obtain Eq. 29,

$$\frac{\partial^2 T}{\partial y^2} \approx \frac{T_{i,j+1}^n + T_{i,j-1}^n - 2T_{i,j}^n}{\Delta y^2} \tag{29}$$

Through the discretization of <u>*t*</u>, the authors were able to obtain Eq. 30,

$$T_{i,j}^{n+1} = T_{i,j}^n + \left[a\left(\frac{T_{i+1,j}^n + T_{i-1,j}^n - 2T_{i,j}^n}{\Delta x^2} + \frac{T_{i,j+1}^n + T_{n,j-1}^n - 2T_{i,j}^n}{\Delta y^2} + \frac{\dot{\Phi}}{\rho c} \right) \right] \Delta t \tag{30}$$

In order to make Eq. 31,

$$\vec{T}_{i,j}^n = \begin{bmatrix} T_{1,1}^n & \cdots & T_{1,N_x+1}^n \\ \vdots & \ddots & \vdots \\ T_{N_y+1,1}^n & \cdots & T_{N_y+1,N_x+1}^n \end{bmatrix} \tag{31}$$

the authors were able to obtain Eq. 32,

$$T^{n+1} = T^n + \left[a\left(\frac{1}{\Delta x^2} \begin{bmatrix} -2 & 1 & & \\ 1 & -2 & \ddots & \\ & \ddots & \ddots & 1 \\ & & 1 & -2 \end{bmatrix} T^n + \frac{1}{\Delta y^2} T^n \begin{bmatrix} -2 & 1 & & \\ 1 & -2 & \ddots & \\ & \ddots & \ddots & 1 \\ & & 1 & -2 \end{bmatrix} + \frac{\dot{\Phi}}{\rho c} \right) \right] \Delta t \tag{32}$$

Boundary conditions

For the second kind of boundary condition, after $\frac{\partial T}{\partial x}\big| x = j = \mu_{i,j}^n$ discretization, the authors could obtain Eq. 33,

$$\frac{\partial T}{\partial x}\bigg| x = j \approx \frac{T_{i,j}^{n+1} - T_{i,j-1}^{n+1}}{\Delta x} \tag{33}$$

namely Eq. 34,

$$\frac{T_{i,j}^{n+1} - T_{i,j-1}^{n+1}}{\Delta x} = \mu_{i,j}^{n+1} \tag{34}$$

Therefore, $T_{i,j}^{n+1} = T_{i,j-1}^{n+1} + \mu_{i,j}^{n+1}\Delta x$, $T_{i,j}^{n+1} = T_{i,j-1}^{n+1} - \mu_{i,j}^{n+1}\Delta x$;
So, $T_{i,1}^{n+1} = T_{i,2}^{n+1} - 0 \cdot \Delta x = T_{i,2}^{n+1}$; $T_{i,N_x+1}^{n+1} = T_{i,N_x}^{n+1} + 0 \cdot \Delta x = T_{i,N_x}^{n+1}$; and $T_{N_x+1,j}^{n+1} = T_{N_x,j}^{n+1} - 0 \cdot \Delta y = T_{N_x,j}^{n+1}$

For the third boundary condition, as shown by Eq. 35,

$$\frac{\partial T}{\partial y}\bigg| y = d = \frac{q_c + q_r}{-\lambda} \tag{35}$$

the authors could obtain Eq. 36,

$$\frac{T_{N_y+1}^{n+1} - T_{N_y,j}^{n+1}}{\Delta y} = \frac{q_c + q_r}{-\lambda} \tag{36}$$

namely Eq. 37,

$$T_{N_y+1}^{n+1} = T_{N_y,j}^{n+1} + \Delta x \cdot \frac{q_c + q_r}{-\lambda} \tag{37}$$

The initial condition was $T_{i,j}^0 = T_0$.

RESULTS AND DISCUSSION

MATLAB Simulation of the Model

Process description of model simulation

For the numerical calculation of heat transfer, MATLAB has a powerful and complete numerical simulation ability, which is suitable for solving this kind of heat transfer differential equation. Therefore, this work made use of MATLAB to carry out programming of the directional control and boundary conditions that had gone through discretization and conducted a simulated calculation for different surface layer thicknesses, heat-accumulating layer thicknesses, and graphene fiber spacings, so as to simulate the thermal-electric performance of a graphene floor in the actual working process.

## Results and Analysis of Model Simulation

According to the established heat transfer model, the authors were able to confirm that the thickness of the floor surface, the thickness of the heat accumulating layer, and the graphene fiber spacing were the primary factors affecting the thermal-electric performance of the graphene floor. In order to obtain the ideal heating effect, the primary parameters of the graphene floor needed to be optimized. According to the thickness of the existing common floor in the market and the requirements set by industry standards, as well as the goals of the overall thickness of the floor not exceeding 18 mm, a high uniformity of plate surface temperature, and the time from the beginning of heating the graphene floor to 90% of the stable working temperature should not be more than 20 min, the authors designed a multi-factor orthogonal experimental design. The factor parameters are shown in Table 2, through the simulation test of all factors, where the temperature of the graphene floor from heating to stable operation, the 90% temperature from heating to stable operation, and the time required were obtained.

Table 2. Parameters List

Graphene fiber spacing	5 mm, 10 mm
Surface thickness	2 mm, 4 mm, 6 mm, 8 mm 10 mm, 12 mm, 14 mm, 16 mm, 18 mm
Thickness of the heat-accumulating layer	0 mm, 2 mm, 4 mm, 6 mm, 8 mm, 10 mm, 12 mm, 14 mm, 16 mm

Through the orthogonal simulation test of the above parameters (as shown in Table 2), in turn, the number of test groups meeting the requirements was 90 in total. The two groups of the response surface obtained from the simulation results are shown in Fig. 5.

As shown in Fig, 5a, when the fiber spacing between the upper and lower surfaces was 10 mm, respectively, the temperature increase could reach the stable working temperature at the floor surface where x = 0 mm and x = 5 mm. However, it could not be seen from Fig. 5 that, with the increase of the thickness of the floor surface, the temperature difference of the plate surface at x = 0 mm was gradually smaller than that at x = 5 mm, which showed a trend of gradually decreasing at first and then basically overlapping. When the thickness of the heat accumulating layer was 0 mm and the thickness of the floor surface was approximately 6 mm, the temperature difference of each point on the floor surface was basically 0. The maximum temperature difference was 0.9 K. As shown in Fig. 4b, when the fiber spacing of the two curved surfaces was 20 mm, the temperature increase of the floor surface where x = 0 mm and x = 10 mm could reach the stable working temperature; the temperature difference still showed a trend of gradually decreasing at first and then basically overlapping. When the thickness of the heat-accumulating layer was 0 mm and the thickness of the surface floor was 2 mm, the temperature difference reached a maximum of 4.3 K. When the thickness of the heat-accumulating layer was 0 mm and the thickness of the floor surface layer was approximately 14 mm, the temperature difference of each point on the floor surface was basically 0. When the fiber spacing increased to 10 mm, the temperature uniformity of the floor surface became poor. It decreased only when the thickness of the surface layer and the heat-accumulating layer increased, accompanied often by an increase in heating time.
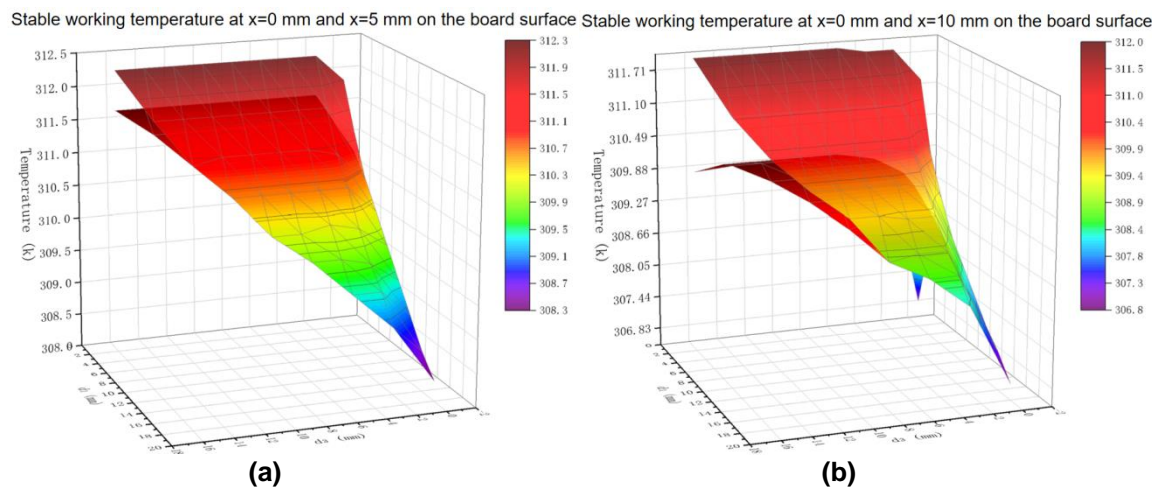
Fig. 5. Fitting data of the response surface

When the thickness of the surface layer remained unchanged and the fiber spacing was 10 mm, with an increase of the thickness of the heat accumulating layer, the stable working temperature at each point of the floor surface could reach the stable working temperature, which showed a trend of increasing first, followed by decreasing, and then remaining unchanged. When the heat-accumulating layer of each layer was 4 mm, the stable working temperature reached the maximum. When the fiber spacing was 20 mm, with the thickness of the heat-accumulating layer increasing, the stable working temperature of each point of the floor surface showed a trend of increasing first, then decreasing, and then remaining unchanged. When the heat-accumulating layer of each layer was 6 mm, the stable working temperature reached the maximum. Therefore, the authors were able to show that when the heat-accumulating layer was set on the graphene electrically heated floor, the storage energy kept releasing heat and the limiting temperature of each point of the floor surface could be effectively increased and the temperature uniformity of the surface plate could be increased.

When the thickness of the heat-accumulating layer remained unchanged, with the increase of the thickness of the surface layer, the wood of the surface layer absorbed more energy, which reduced the energy that was transferred to the floor surface, leading to the stable working temperature of each position of the floor surface to decrease with the thickness increase of the surface layer.

Figure 6 shows that when the fiber spacing was 10 mm, the temperature of the floor surface reaching 90% of the stable work was a little higher, and the time needed for the temperature increase was greatly decreased, compared with the situation when the fiber spacing was 20 mm. When the thickness of the surface layer was relatively small, with an increase in the heat-accumulating layer, it could act as the bottom heat conducting medium, leading to the faster temperature increase. However, with the increase of the fiber spacing, the requirement for the thickness of the heat-accumulating layer also increased. According to GB-T / 4654-2008 General Specification for Infrared Radiation Heater with Non-metallic Substrate, the time from the beginning of heating to 90% of the stable working temperature of the heating surface should not exceed the requirement of 20 min. When the fiber spacing was 10 mm, 38 groups (84.4%) met the requirements, while when the fiber spacing was 20 mm, only 11 groups (24.4%) met the requirements.
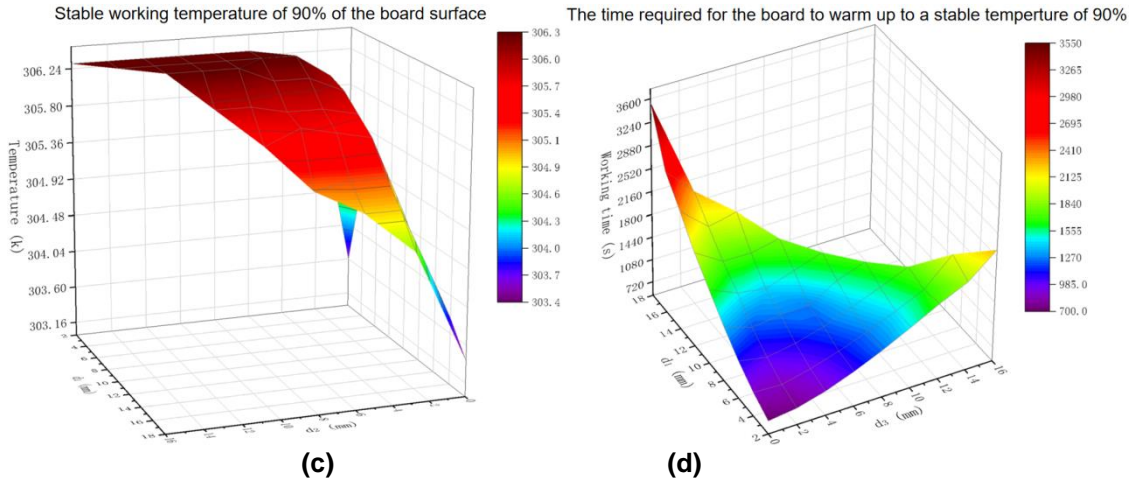

(a)   (b)
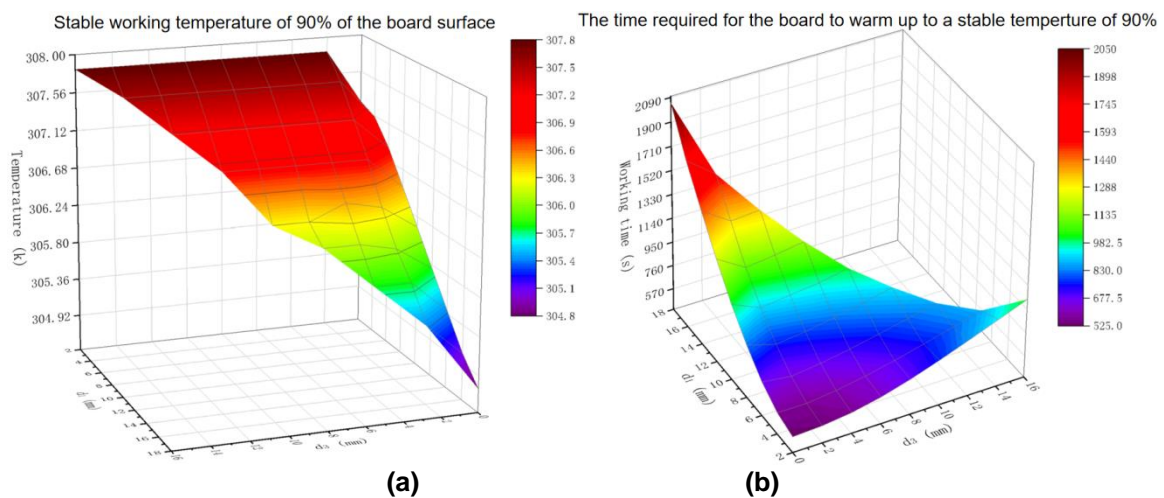
Fig. 6. Variation of the temperature field under different panel thicknesses

Simulation of the Heat Storage Performance of the Model

Due to the presence of the energy storage layer, the floor could continuously distribute the energy stored during power on to the outside when it was powered off after heating for a period of time. Therefore, the heat storage performance was also an important factor to be considered in graphene floor design. Based on previous research, the experimental group with a fast-heating time and high stable temperature was comprehensively selected from the heating time in line with the national standard to continue the simulation test of the heat storage performance. The experimental groups participating in the thermal storage performance simulation are shown in Table 3.

Table 3. Simulation Experiment Data

Serial Number	Thickness of the Surface Layer (mm)	Thickness of the Heat-Accumulating Layer (mm)	Temperature for Stable Working (K)	Stable Working Temperature and Heating Time (S)	Temperature for 90% of the Stable Work (K)	Heating time of the Temperature for 90% of the Stable Work (s)
1	2	0	311	812.1	307.2	527.3
2	2	2	311.7	807.7	307.83	538.9
3	2	4	311.7	919.6	307.83	567.8
4	4	0	310.9	933.5	307.11	571.9
5	4	2	311.4	891	307.56	571.1
6	4	4	311.4	983.5	307.56	598.8

In order to better simulate the actual working process, after people turned on the floor for a period of time, the temperature of the environment was initially increased. Then people disconnected the power supply to bring the residual temperature in the floor heat the environment to a comfortable temperature. Therefore, the heat storage performance test was divided into two steps: first, people made the heat source in the model simulate the power on working state within the first 20 min; and second, made the heat source in the

model simulate the power off working state within the last 20 min. The simulation results are shown in Fig. 7.
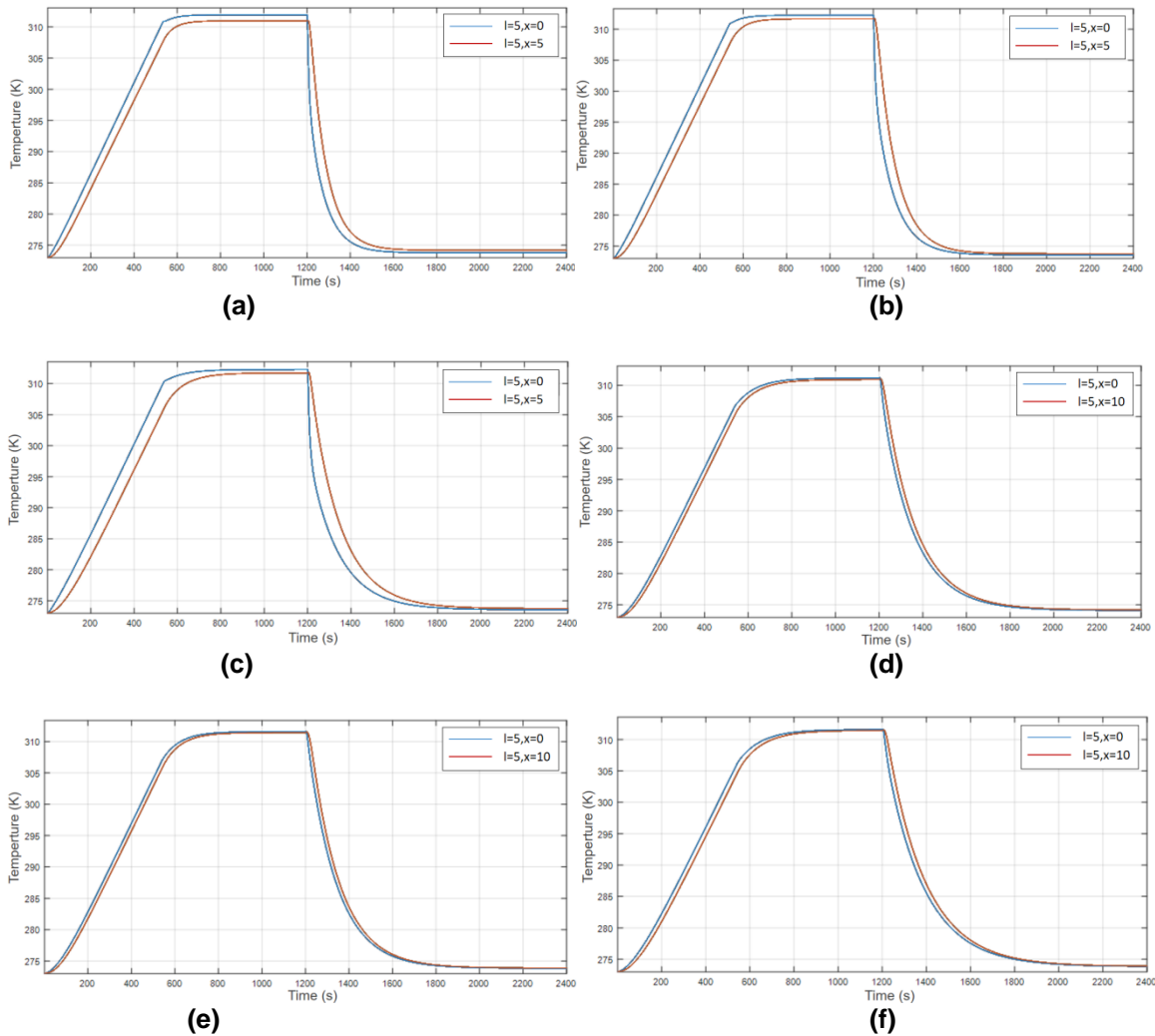

Fig. 7. Heat storage performance test curve

As shown in Fig. 6, 6a through 6f were test groups 1 through 6, respectively. Parts 6a, 6b, and 6c, with a surface thickness of 2 mm, showed obvious temperature heterogeneity in both the heating and heat-accumulating layer. Compared with Fig. 6d and 6f, Fig. 6E, with a 4 mm surface layer, had obvious advantages in terms of the heating rate, heat storage rate, and temperature uniformity. Through the MATLAB goodness of fit solution, the authors determined that $R^2_a = 0.9921$; $R^2_b = 0.9723$; $R^2_c = 0.9436$; $R^2_d = 0.9974$; $R^2_e = 0.9981$; and $R^2_f = 0.9970$. Therefore, it was considered that the optimal distance between the graphene fibers was 10 mm, the optimal thickness of the surface layer was 4 mm, and the optimal thickness of the heat accumulating layer was 2 mm.

Experimental Analysis and Comparison

In this article, the optimal group from the comprehensive performance in the heat storage simulation calculation was selected for testing. The test environment was consistent with the initial conditions of the differential equation. Drawing the temperature curve and

comparing the simulation results was aimed at verifying the correctness of the mathematical model and simulation calculation.

Experimental Materials

The test time in this article was in Harbin an unheated warehouse. The outdoor temperature was -2 °C and the temperature in the test area was 0 °C .

Phenolic resin (PF) adhesive produced by Dynea was selected, whose primary performance parameters are shown in Table 4.

Table 4. The Primary Performance Parameters of the Phenolic Resin

Viscosity (18 °C)	Solid Content	pH Value
93 MPa·s	44.5%	12.05

The resin content was 15%, the hot-press temperature was 135 °C, and the hot-press time was 2 min/mm. According to the above design parameters, the materials of each layer were arranged in a criss-cross manner and pressed. The obtained floor was placed outdoors for 2 days to eliminate any internal stress to make the floor temperature consistent with the ambient temperature. The dimensions and materials of each floor layer are shown in Table 5.

Table 5. Materials and Dimensions of Each Layer of the Experimental Floor

Names of each Layer	Materials	Breadth	Thickness
Surface floor	Walnut veneer	50mm × 13.5mm	4 mm
Heating layer	Graphene heating layer	50mm × 13mm	1 mm
Thermal barrier	Alumina-silicate ceramic fibre thermal barrier	50mm × 13.5mm	1.5 mm
Reflective coating	Aluminum foil reflective coating	50mm × 13.5mm	0.5 mm
Substrate layer	Aspen wood base material	50mm × 13.5mm	9 mm
Bottom layer	Aspen wood veneer	50mm × 13.5mm	2 mm

In order to avoid strong convective heat transfer on the floor surface caused by airflow interference, the test piece was placed above the self-made test box on the floor. A contact temperature sensor was arranged in the center of the test chamber, which could monitor the surface temperature change of the test piece in real time, with the accuracy of the sensor being 0.1 °C.

Contrast Experiment

Fabrication of the floor test piece

The walnut veneer, aspen wood veneer, and aspen wood base material were comprehensively crisscrossed. The graphene heater and the reflective thermal barrier were set between the walnut veneer and aspen wood veneer, the aspen wood veneer, and aspen wood base material. The resin content of a single side was 90 g/m^3. After placed for 20 min after sizing, the test piece was put between the upper and lower pressing plates of the hot press. The hot-pressing temperature was set to 135 °C and the hot pressing time was set to 2 min/mm. After pressing and molding, the sample should be aged for 24 h to

eliminate internal stress. The floor test piece was shown in Fig. 8a, while the test equipment is shown in Fig. 8b.

(a)   **(b)**

Fig. 8. Test piece of the floor (a); and test temperature measuring device (b)

The floor was then placed in a customized box of 1 m. The temperature monitoring points were reasonably selected to verify the temperature increase effect of the floor on the space, so as to obtain the heat transfer efficiency and energy storage effect of the floor.

Thermal-electric performance test

The groups with the best comprehensive performance, *i.e.*, the thickness of the surface layer was 4 mm, and the thickness of the heat-accumulating layer was 2 mm, in the heat storage simulation calculation were selected to test the thermal-electric performance. According to the requirements of GB / T 7287-2008 Experimental Method of Infrared Radiation Heater, 9 temperature measurement points were divided on the floor surface. In addition, it was ensured that the test environment was consistent with the initial conditions of the differential equation. In order to avoid the strong convective heat transfer on the surface of the pressed graphene composite floor caused by airflow interference, the floor test piece was placed in the self-made test box with an upper opening during the experiment. The power supply was turned on for 20 min and then turned off for 20 min. The temperature sensors were used during contact to measure the temperature change of each temperature measuring point. The temperature of 9 temperature measuring points were measured at a time interval of 10s, according to Eq. 38,

$$\bar{T} = \frac{1}{9}\sum_{i=1}^{9} T_i \tag{38}$$

followed by calculating the average temperature and drawing the temperature curve, as shown in Fig. 9.

Figure 10 shows that the trend of the measured temperature data was generally consistent with the simulation calculation. When the maximum difference was 1200 s, the floor temperature of the test was up to 310.4 K, which was only a 3.2% different from the simulated value 311.6 K, which verified the correctness, the advanced nature, and predictability. The model could provide strong guidance for the manufacture and selection of graphene electrically heated floors and the prediction of the temperature increase.
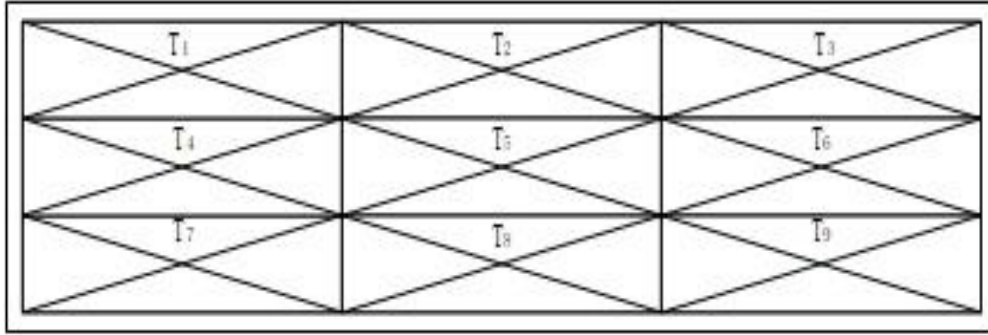
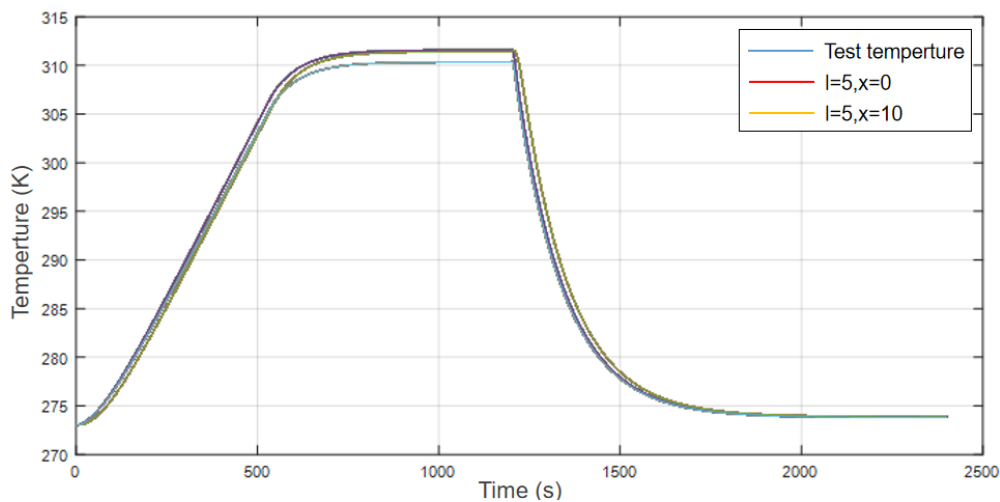**Fig. 9.** Division of temperature measuring points

Fig. 10. Comparison between the test temperature curve and the calculated temperature curve

CONCLUSIONS

1. This article presented a calculation model which could be used to describe the stable heating process of electrically heated floors. Using this model, the heating time and limit temperature of any point on the floor surface of the related products could be accurately and conveniently calculated, which provided new guidance for the preliminary research in the electric heating floor industry and the selection of the thickness of the non-functional layer.

2. Through model calculation and test verification, the results showed the following: the heating process of the graphene floor showed an exponential change law. The difference between the heating time and the termination temperature obtained by the two methods was no greater than 3.2%.

3. The position of the heating layer and the spacing of the graphene heating fiber had a certain influence on the limit temperature, heating time, and temperature distribution uniformity. With the increase of the thickness of the surface layer, the heat accumulating layer, and the spacing of the heating fiber, the limit temperature that could be reached by the plate surface gradually decreased and the time needed to heat up to a stable temperature gradually increased. However, with the decrease of the

heating fiber spacing, the uniformity of the temperature distribution gradually improved.

4. Through simulation calculation and test detection, this article selected a spacing of graphene heating fiber with a thickness of 10 mm, a thickness of the floor surface of 4 mm, and a thickness of the heat-accumulating layer of 2 mm. In this situation, the thermal-electric performance was optimal.

5. The floor boasted good heat transfer performance, which took 333 min to increase the temperature from 17.9 to 41.53 °C in an enclosed space.

ACKNOWLEDGEMENTS

REFERENCES CITED

Al-Mashaal, A. K., Wood, G. S., Torin, A., Mastropaolo, E., Newton, M. J., and Cheung, R. (2017). "Dynamic behavior of ultra large graphene-based membranes using electrothermal transduction," *Applied Physics Letters* 111(24), 243503.1-243503.4. DOI: 10.1063/1.5007327

Cao, Z. B., Liu, X. P., Du, G. Y., Chu, X., Liu, D. W., and Zhou, Y. C. (2018). "Temperature prediction model of heat storage of wooden flooring for ground with heating system based on TWSVM and Fuzzy," *Scientia Silvae Sinicae* 54(11), 45-52.

Chen, L., Zhang, Y., and Wu, Q. (2017). "Effect of graphene coating on the heat transfer performance of a composite anti-/deicing component," *Coatings* 7(10), 158. DOI: 10.3390/coatings7100158

Chen, Y.N., Fu, K., Zhu, S. Z., Luo, W., Wang, Y. B., Li, Y. J., Hitz, E., Yao, Y. G., Dai, J. Q., Wan, J., *et al.* (2016). "Reduced graphene oxide films with ultrahigh conductivity as Li-ion battery current collectors," *Nano Letters* 16(6), 3616-3623. DOI: 10.1021/acs.nanolett.6b00743

Du, G. Y., Zhou, S. Y., Liu, D. W., and Zhou, Y. C. (2018). "Technology to detect heat storage efficiency of solid wood flooring for ground with heating system," *Scientia Silvae Sinicae* 54(11), 7-13. DOI: 10.11707/j.1001-7488.20181102

Echeberria, J., Rodriguez, N., Vleugels, J., Vanmeensel, K., Reyes-Rojas, A., Garcia-Reyes, A., Domınguez-Rios, C., Aguilar-Elgue´Zabal, A., and Bocanegra-Bernal, M. H. (2012). "Hard and tough carbon nanotuber-reinforced zirconia-toughened alumina prepared by spark plasma sintering," *Carbon* 50(2), 706-717. DOI: 10.1016/j.carbon.2011.09.031

GB/T-18103 (2013). "Solid wood composite floor," China National Standardization Administration Committee, Beijing.

GB/T-7287 (2008). "Test methods for infrared radiant heaters," China National Standardization Administration Committee, Beijing.

González, B., and Prieto, M. M. (2021). "Radiant heating floors with PCM bands for thermal energy storage: A numerical analysis," *International Journal of Thermal Sciences* 162, 106803. DOI: 10.1016/j.ijthermalsci.2020.106803

Hauser, G., Kempkes, C., and Olesen, B. W. (2000). "Computer simulation of hydronic heating/cooling system with embedded pipes," *ASHRAE Transactions* 106(1), 702-710.

Li, S. C. (2018). *Study on Structure Design and Heat Transfer Performance of Electric Composite Floor with Built-in Electrothermal Layer*, Ph.D. Dissertation, Beijing Forestry University, Beijing, China.

Liu, C. G., Zhou, S. Y., Ge, Z. D., Du, G. Y., and Zhou, Y. C. (2018). "The construction and verification of heat storage performance testing model of wood materials used for floor heating," *Scientia Silvae Sinicae* 54(10), 125-131. DOI: 10.11707/j.1001-7488.20181015

Liu, D., Du, G. Y., Chu, X., Cao, Z. B., Liu, X. P., and Zhou, Y. C. (2018). "Real-time parallel acquisition method for temperature field of wooden floor heat storage performance," *Scientia Silvae Sinicae* 54(11), 180-186. DOI: 10.11707/j.1001-7488.20181125

Liu, G. (2017). *Preparation and Electrothermal Properties of Graphite Nanosheet Composite Films*, Master's Thesis, Harbin Institute of Technology, Harbin, China.

Lu, J. (2001). *MATLAB solution of partial differential equation*, Wuhan University Publisher, Wuhan, China.

Luo, J. F., Gang, Z., Li, Y. Q., and Zhi, C. F. (2012). "The differential thermal analysis on several kinds of wooden floor," *Fire Science and Technology* 31(03), 234-236.

Shi, J. Y. (2007). *Heat Transfer Simulation of Low-Temp Hot Water Radiant Floor Heating,* Harbin Institute of Technology, Master's Thesis, Harbin, China.

Song, Y. Q. (2019). *Construction of Three-Dimensional Graphene Materials and their Applications in Supercapacitors and Electrothermal Films*, China University of Science and Technology, Ph.D. Dissertation, Hefei, China.

Vivekchand, S. R. C., Rout, C. S., Subrahmanyam, K. S., Govindaraj, A., and Rao, C. N. R. (2008). "Graphene-based electrochemical supercapacitors," *Journal of Chemical Sciences* 120(1), 9-13.

Wang, R., Xu, Z., Zhuang, J. H., Liu, Z., Peng, L., Li, Z., Liu, Y. J., Gao, W. W., and Gao, C. (2017). "Highly stretchable graphene fibers with ultrafast electrothermal response for low-voltage wearable heaters," *Advanced Electronic Materials* 3(2), article 1600425. DOI: 10.1002/aelm.201600425

Wei, H. L., Mazumder, J., and Debroy, T. (2015). "Evolution of solidification texture during additive manufacturing," *Scientific Reports* 5, article 16446.

Yang, W., Zhang, Y., and Wang, R. G. (2001). "Numerical study on heat transfer of the radiant floor heating system," *Heating, Ventilating & Air Conditioning* 31(1), 73-75.

Ye, C. S. (2006). "Application of MATLAB in analysis of stead state and unsteady state heat conduction," *Computer and Applied Chemistry* 23(10), 986-990.

Zhang, C. B., Han, Q., and Chen, Y. P. (2020). "Design of virtual simulation experiment platform for heat transfer course based on MATLAB," *Experimental Technology and Management* 37(01), 132-136.

Zhang, Y. B., Lu, C. L., and Jin, S. M. (2012). "The research of floor heat transfer characteristic in floor heating," *Chinese Academy of Engineering*, *Zhejiang Science and Technology Association*, 2005, 5.

Zhou, S. Y., Du, G. Y., Cao, Z. B., Liu, X. P., and Zhou, Y. C. (2018). "Measurement and inverse prediction methods of heat storage performance for wood flooring with geothermal system," *Scientia Silvae Sinicae* 54(11), 14-19.